A two-phase flow model for submarine granular flows: With an application to collapse of deeply-submerged granular columns

Cheng-Hsien Lee[c], Zhenhua Huang[d,*]

[a]*Department of Water Resources and Environmental Engineering, Tamkang University, Taiwan*
[b]*Department of Ocean and Resources Engineering, School of Ocean and Earth Science and Technology, University of Hawaii at Manoa, Honolulu HI 96822, USA*

Abstract

The collapse process of a submerged granular column is strongly affected by its initial packing. Previous models for particle response time, which is used to quantify the drag force between the solid and liquid phases in rheology-based two-phase flow models, have difficulty in simulating the collapse process of granular columns with different initial concentrations (initial packing conditions). This study introduces a new model for particle response time, which enables us to satisfactorily model the drag force between the two phases for a wide range of volume concentration. The present model can give satisfactory results for both loose and dense packing conditions. The numerical results have shown that (i) the initial packing affects the occurrence of contractancy/diltancy behavior during the collapse process, (ii) the general buoyancy and drag force are strongly affected by the initial packing through contractancy and diltancy, and (iii) the general buoyancy and drag force can destabilize the granular material in loose packing condition but stabilize the granular material in dense packing condition. The results have shown that the collapse process of a densely-packed granular column is more sensitive to particle response time than that of a loosely-packed granular column.

Keywords: Numerical simulation, Two-phase flow model, Particle response time, Granular flow, Initial packing condition, Landslide

*Corresponding author contacts:
Email address: zhenhua@hawaii.edu (Zhenhua Huang)

A two-phase flow model for submarine granular flows: With an application to collapse of deeply-submerged granular columns

Cheng-Hsien Lee[c], Zhenhua Huang[d,*]

[c]*Department of Water Resources and Environmental Engineering, Tamkang University, Taiwan*
[d]*Department of Ocean and Resources Engineering, School of Ocean and Earth Science and Technology, University of Hawaii at Manoa, Honolulu HI 96822, USA*

1. Introduction

Submarine landslides may occur on continental margins and slopes (Masson et al., 2006). The ability to accurately simulate submarine landslides has practical importance because the sediment volumes released by submarine landslides may damage submarine cables and other subsea facilities (Hsu et al., 2008). To understand the fundamental physics involved in landslides on land or submarine landslides, the collapse of a granular column has often been used in the past as an idealized model for studying landslides in both laboratory experiments (Lajeunesse et al., 2004, 2005; Lube et al., 2004, 2007, 2005) and discrete element simulations (Zenit, 2005; Girolami et al., 2012; Lacaze et al., 2008). Most of these studies focused on dry granular columns in either two dimensional (2D) (Lajeunesse et al., 2005; Lube et al., 2005) or axisymmetric (Lajeunesse et al., 2004, 2005; Lube et al., 2004, 2007) geometries.

For landslides on land, which involve the collapse of dry granular materials, the granular flow is a solid-air two-phase flow. In the laboratory experiment using a 2D geometry, the granular material is initially confined by two vertical walls; the collapse of the granular column starts when the front wall is suddenly removed. In the laboratory experiment using an axisymmetric geometry, the granular material is initially inside a standing cylinder, and the collapse of the granular column starts when the cylinder is suddenly lifted up. After the wall or the cylinder has been removed, the granular material spreads out and eventually stops moving due to internal friction. Because the density of the air is about 1000 times smaller than the density of the granular material (e.g., sand), the particle-particle interaction dominates the dynamics of the dry granular flow, and the flow dynamics and the deposit morphology depend primarily on the initial aspect ratio of the granular column (Lajeunesse et al., 2004, 2005; Lube et al., 2004, 2007, 2005). The normalized runout has been found to be a power-law function of the initial aspect ratio (Lajeunesse et al., 2004, 2005; Lube et al., 2004, 2007, 2005). For a 2D geometry, the deposit morphology can be either triangular-shaped or trapezoid-shaped, depending on the initial aspect ratio (Lajeunesse et al., 2004). Other factors such as basal and internal frictions play insignificant roles (Lube et al., 2004).

For the collapse of a submerged granular column, the granular flow is a solid-liquid two-phase flow. Because the densities of the liquid (e.g., water) and granular material have the same order of magnitude, the particle-fluid interaction provides additional forces important to the dynamics of the granular flow: the drag force between the particle and the fluid decreases the kinetic energy of the granular flow, and the lubrication force (Rognon et al., 2011) reduces the chance of surface contact among particles. These two types of forces have significant effects on the rheological characteristics of submerged granular flows, especially when a granular flow involves small particles (Boyer et al.,

*Corresponding author contacts:
Email address: zhenhua@hawaii.edu (Zhenhua Huang)

2011; Cassar et al., 2005; Trulsson et al., 2012); this is because the variation of the pore pressure in the granular flow can either stabilize or destabilize the granular material (Iverson et al., 2000).

Unlike in dry and dense granular flows where the initial volume fraction plays no significant role (Lagrée et al., 2011; Ionescu et al., 2015; Lee et al., 2015a), the initial volume fraction is very important for the collapse of submerged granular columns. This is because the dilatancy (if initially over-consolidated) or contractancy (if initially under-consolidated) behavior (Campbell, 2006) can induce a relative motion between the solid grains and the liquid, which in turn can induce an additional force on the granular skeleton and affect the flow (Pailha et al., 2008). For the collapse of a submerged granular column, a previous study using a 2D discrete-element method (Topin et al., 2012) suggests that the combined effect of the drag and lubrication may either reduce or enhance the runout distance. Experiments (Rondon et al., 2011; Bonnet et al., 2010) have found that the initial volume fraction has a significant effect on the collapse of a submerged granular column: for an initially-loose packing, the collapse process is rapid and the deposition layer is thin and long; for an initially-dense packing, the collapse process is slow and the runout distance is much shorter (Rondon et al., 2011).

Rondon et al. (2011) conjecture that the dilatancy or contractancy behavior plays an important role in the collapse process. The conjecture of Rondon et al. (2011) is described below:

1. For an initially-loose packing, the granular column first contracts locally when the column starts to collapse; at the initial stage, a high pore-pressure zone forms inside the column, causing some pore water to flow out which helps to destabilize the granular material near the surface.
2. For an initially-dense packing, the granular column will first dilate when the granular column starts to collapse. At the initial stage, a low pore-pressure zone forms inside the granular column, causing the water to be absorbed into the granular material which helps to stabilize and the granular material near the surface.

However, this conjecture has not been proved by either experimental measurements or numerical simulations. It is also not clear how the dilatancy and contractancy behaviors affect the interfacial forces.

Many continuum models (Lagrée et al., 2011; Ionescu et al., 2015; Lee et al., 2015a) have been proposed in the past to simulate the collapse of incompressible dry granular columns. Because the dilatancy and contractancy behaviors affect the pore pressure in the collapse process of a submerged granular column, the existing models developed for dry granular materials may not be suitable for submerged granular columns. Meruane et al. (2010) first developed a two-phase model to simulate the collapse of a submerged granular column, which was later extended by Meruane et al. (2012) to deal with granular flows of binary mixtures of particles. However, Meruane et al. (2010, 2012) used a combination of Coulomb friction and the kinetic theory to develop their constitutive model for solid-phase stress, which needs to be modified for high concentration flows. Furthermore, Meruane et al. (2010, 2012) did not study the effect of the initial volume fraction on the collapse. Savage et al. (2014) proposed a mixture model to study the collapse of a submerged granular column and examined both the initially-loose and dense packings; however, their model neglects the pore pressure and the interaction between the particles and interstitial fluid, and thus cannot reproduce the flow behavior observed in the collapse of submerged granular columns. We are not aware of any models in the literature that are suitable for simulating the collapse of submerged granular columns with different initial packing conditions.

Using a new rheological characteristics for high concentration flows, Lee et al. (2016) extended the model of Lee et al. (2015a), which was developed for the collapse of dry granular columns, to study solid-liquid two-phase flows where the packing of the solid phase is not dense. We have tried to use the model of Lee et al. (2016) to simulate the collapse of submerged granular columns, but the results for the initially-dense packing are not satisfactory when compared with the experimental results of Rondon et al. (2011). We conjectured that the parametrization of particle response time adopted in Lee et al. (2016) might have contributed to the difference between the numerical and

experimental results; this is because the particle response time τ_p, which is used to parametrize the drag force between the two phases, affects the dissipation of high/low pore pressure built up in the granular material (Das, 2013). The particle response time in Lee et al. (2016) was computed using the terminal velocity of a particle with a concentration correction proposed by Richardson and Zaki (1954); however, this model may not be suitable in very high concentration regions where the contact among particles prevents the particles to freely fall. We have also tried to compute the particle response time based on the pressure drop in steady flows through a homogenous porous media (Engelund, 1953); however, this model cannot yield satisfactory results for initially-dense packing condition as well. For reference, the collapse processes simulated by using the models of Richardson and Zaki (1954) and Engelund (1953) are included in Appendix A.

For very high concentrations, Camenen (2005) further modified the concentration correction of Richardson and Zaki (1954); but the model of Camenen (2005) is singular close to the maximum concentration at which contact networks form. In this study, we introduce a new model for particle response time to compute the drag force in submerged granular flows. The new model combines the concentration correction of Camenen (2005) to the terminal velocity with a limiter derived from the model of Engelund (1953). One of the main objectives of this study is to find a new model for particle response time that can work for both initially loose and dense packing conditions. The performance of the new model is evaluated by comparing the numerical results, obtained by the new model and two existing models, with the experimental results of Rondon et al. (2011).

2. Model descriptions

For completeness and later discussion, the governing equations and main constitutive models are briefly presented first, followed by a description of three models for particle response time.

2.1. Governing equations

For the two-phase model used in this study, the equations governing the fluid and solid phases are obtained by taking two averages over the microscopic governing equations for each phase (Hsu et al., 2003). The resulting equations governing the conservation of mass and momentum are

$$\frac{\partial \rho_f (1-c)}{\partial t} + \nabla \cdot [\rho_f (1-c)\mathbf{u}^f] = 0, \tag{1}$$

$$\begin{aligned} &\frac{\partial \rho_f (1-c)\mathbf{u}^f}{\partial t} + \nabla \cdot [\rho_f (1-c)\mathbf{u}^f \mathbf{u}^f] = \\ &\rho_f (1-c)\mathbf{g} - (1-c)\nabla p_f + \nabla \cdot [(1-c)\mathbf{T}^f] \\ &- \left\{ c\rho_s \frac{\mathbf{u}^f - \mathbf{u}^s}{\tau_p} - \frac{\rho_s}{\tau_p} \frac{(1-c)\nu_{ft}}{\sigma_c} \nabla c \right\}, \end{aligned} \tag{2}$$

for the fluid phase, and

$$\frac{\partial \rho_s c}{\partial t} + \nabla \cdot (\rho_s c \mathbf{u}^s) = 0, \tag{3}$$

$$\begin{aligned} &\frac{\partial \rho_s c\mathbf{u}^s}{\partial t} + \nabla \cdot (\rho_s c \mathbf{u}^s \mathbf{u}^s) \\ &\quad = \rho_s c g - c\nabla p_f - \nabla (c p_s) + \nabla \cdot (c\mathbf{T}^s) \\ &\quad + \left\{ c\rho_s \frac{(\mathbf{u}^f - \mathbf{u}^s)}{\tau_p} - \frac{\rho_s}{\tau_p} \frac{(1-c)\nu_{ft}}{\sigma_c} \nabla c \right\}, \end{aligned} \tag{4}$$

for the solid phase. In these equations, ρ_f and ρ_s are the mass densities of the fluid and solid phases, respectively; c is the solid volume friction (i.e., concentration); $\mathbf{u}^f$ and $\mathbf{u}^s$ are the mean velocities of

the fluid and solid phases, respectively; $\mathbf{g}$ is the acceleration due to gravity; p_f is the total pressure of the fluid phase (or pore pressure in this study); p_s is the pressure of the solid phase; $\mathbf{T}^f$ and $\mathbf{T}^s$ are the stresses of the fluid and solid phases, respectively; τ_p is the particle response time used to parameterize the inter-phase drag force; ν_{ft} is the eddy viscosity of the fluid phase; σ_c is the Schmidt number. The term $-c\nabla p_f$ in Eq. (4) is the pressure force of the fluid phase and referred to as general buoyancy in the literature (Meruane et al., 2010). The two terms in the curly-brackets in Eqs. (2) and (4) are related to the inter-phase momentum transfer.

A $k-\epsilon$ model with a low-Reynolds-number correction is adopted to compute $\mathbf{T}_f$ (Lee et al., 2016). The turbulence kinetic energy k and its dissipation rate ϵ are governed by

$$\begin{aligned}
&\frac{\partial \rho_f(1-c)k}{\partial t} + \nabla\cdot[\rho_f(1-c)\mathbf{u}^f k] \\
&= (1-c)\mathbf{T}^f : \nabla\mathbf{u}^f - \rho_f(1-c)\epsilon \\
&+ \nabla\cdot[\rho_f\frac{\nu_{ft}}{\sigma_c}(1-c)\nabla k] \\
&- \left\{(\rho_s-\rho_f)\frac{(1-c)\nu_{ft}}{\sigma_c}\nabla c\cdot\mathbf{g} + \frac{2\rho_s c(1-\alpha)k}{\tau_p}\right\},
\end{aligned} \tag{5}$$

and

$$\begin{aligned}
&\frac{\partial \rho_f(1-c)\epsilon}{\partial t} + \nabla[\rho_f(1-c)\mathbf{u}^f\epsilon] = \\
&\frac{\epsilon}{k}[C_{\epsilon1}f_1(1-c)\mathbf{T}^f : \nabla\mathbf{u}^f - C_{\epsilon2}f_2\rho_f(1-c)\epsilon] \\
&+ \nabla\cdot\left[\rho_f\frac{\nu_{ft}}{\sigma_\epsilon}(1-c)\nabla\epsilon\right] \\
&- \frac{\epsilon}{k}C_{\epsilon3}\left\{(\rho_s-\rho_f)\frac{(1-c)\nu_{ft}}{\sigma_c}\nabla c\cdot\mathbf{g} + \frac{2\rho_s c(1-\alpha)k}{\tau_p}\right\},
\end{aligned} \tag{6}$$

where $C_{\epsilon1}$, $C_{\epsilon2}$, σ_ϵ, σ_k , f_1 and f_2 are model parameters. The adopted values for these parameters are the same as those in the $k-\epsilon$ model for clear fluid under low Reynolds number conditions (Launder and Sharma, 1974). The two terms inside the curly brackets in Eqs. (5) and (6) account for the turbulence modulation due to the presence of particles. The first term is associated with the general buoyancy, and the second term is due to the correlation of the fluctuating velocities of solid (sediment) and fluid phases. At present, the value of $C_{\epsilon3}$ is not well understood, and $C_{\epsilon3}=1$ is adopted here as in the previous study (Lee et al., 2016). A sensitivity analysis of the numerical results to $C_{\epsilon3}$ will be given later. The parameter α reflects the correlation between the sediment and fluid turbulent motions and is given by

$$\alpha = \left(1+\frac{\tau_p}{min(\tau_l,\tau_c)}\right)^{-1}, \tag{7}$$

with $\tau_l = 0.165k/\epsilon$ being the time scale of the turbulent flow and τ_c the time scale of particle collisions (Lee et al., 2016).

Strictly speaking, the presence of sediment in turbulent flow may enhance (for large particles) or reduce (for small particles) the turbulence (Crowe, 2000), but Eqs. (5) and (6) can only reflect the reduction of turbulence. Other turbulence models (Crowe, 2000; Lee et al., 2015b) include a term describing the enhancement of turbulence; however, we have found including that term in the present model may induce numerical instability.

2.2. Pressure and stress of the solid phase

We follow Lee et al. (2016) to compute p_s and $\mathbf{T}^s$. In order to cover various sediment transport regimes, Lee et al. (2016) combined the constitutive relations that are applicable to dilute flows,

dense flows, and compact beds. Accordingly, p_s includes three components:

$$p_s = p_{st} + p_{sr} + p_{se}, \tag{8}$$

where p_{st} accounts for the turbulent motion of sediment particles, which is important for dilute flows; p_{sr} reflects the rheological characteristics for dense flows and it includes the enduring-contact, particle inertial, and fluid viscosity effects; p_{se} accounts for the elastic effect important when sediment is static in a compact bed. The shear stress tensor for the sediment phase is computed by

$$\mathbf{T}^s = -\left(\frac{2}{3}\rho_s\nu_s\nabla\cdot\mathbf{u}^s\right) + 2\rho_s\nu_s\mathbf{D}^s, \tag{9}$$

where ν_s is the kinematic viscosity and $\mathbf{D}^s$ the tensor of strain rate. To consider both the turbulence behavior (for dilute flows) and the visco-plastic behavior (for dense flows and compact beds), ν_s is divided into two components:

$$\nu_s = \nu_{st} + \nu_{sv}, \tag{10}$$

where ν_{st} and ν_{sv} represent the turbulence and visco-plastic effects, respectively.

An analysis of heavy and small particles in homogeneous steady turbulent flows (Hinze, 1959) suggests that p_{st} and ν_{st} can be expressed as (Eq. 5-207 and Eq. 5-209 in Hinze (1959))

$$p_{st} = \frac{2}{3}\rho_s\alpha k, \tag{11}$$

and

$$\nu_{st} = \alpha\nu_{ft}. \tag{12}$$

For sediment in a compact bed, the formula proposed by Hsu et al. (2004) is adopted to compute p_{se},

$$\begin{aligned} p_{se} = {} & K[\max(c-c_o,0)]^{\chi} \\ & \left\{1+\sin\left[\max\left(\frac{c-c_o}{c_{rcp}-c_o},0\right)\pi-\frac{\pi}{2}\right]\right\}, \end{aligned} \tag{13}$$

where c_{rcp} = random close packing fraction; c_o, K and χ are model parameters. Obviously, K is associated with Young's modulus and the other terms are related to material deformation.

For dense flows, the visco-plastic rheological characteristics highly depend on a combined dimensionless parameter, $I = I_v + aI_i^2$, where I_v is the viscous number, I_i is the inertial number, and a is a constant (Trulsson et al., 2012). The viscous number describes the ratio of the viscous stress to the quasi-static shear stress associated with the weight (resulting from the enduring contact), and it is defined by $I_v = 2\rho_f\nu_f D^s/cp_s$ where ν_f = the kinematic viscosity of the fluid, D^s = the second invariant of the strain rate, and d = the particle diameter. The inertial number, defined by $I_i = 2dD^s/\sqrt{cp_s/\rho_s}$, describes the ratio of the inertial stress to the quasi-static stress. The relative importance of the inertial number to the viscous number in the dimensionless parameter I can be measured by the Stokes number $st_v = I_i^2/I_\nu$. Some formulas have been proposed to describe $c-I$ and $\eta-I$ relationships, where $\eta = T^s/p_s$ with T^s being the second invariant of $\mathbf{T}^s$. Trulsson et al. (2012) proposed

$$\eta = \eta_1 + \frac{\eta_2-\eta_1}{1+I_o/I}, \tag{14}$$

where η_2 and I_o are constants and $\eta_1 = \tan\theta_s$ with θ_s = the angle of repose. Following the work of Boyer et al. (2011), Lee et al. (2016) assumed

$$c = \frac{c_c}{1+bI^{1/2}} \tag{15}$$

where c_c is a critical concentration representing the maximum packing fraction of an homogeneously sheared assembly of frictional spheres (Boyer et al., 2011) and b is a model parameter. Eq. (15)

implies that c must be smaller than c_c at all time in two-phase flow simulations, which means that c_i, the volume fraction of the initial packing in the simulation, must be smaller than c_c; in other words, the granular material does not behave like a frictional flow before c is internally adjusted to a value slightly smaller than c_c. Boyer et al. (2011) have pointed out that c_c significantly differs from the random-close packing volume fraction and is not sensitive to the initial packing. According to Campbell (2006), c_c can be either larger or smaller than that of the initial packing because of the way it is defined and measured.

Based on Eqs. (14) and (15), Lee et al. (2016) suggested

$$p_{sr} = \frac{2b^2 c}{(c_c - c)^2}(\rho_f \nu_f + 2a\rho_s d^2 D^s)D^s, \tag{16}$$

where b is a constant and

$$\nu_{sv} = \frac{(p_{sr} + p_{se})\eta}{2\rho_s D^s}, \tag{17}$$

Eq. (17) considers sediment in its static state as a very viscous fluid. Because Eq.(15) ensures that c is always smaller than c_c, there is no singularity in Eq. (16) caused by $c = c_c$ in our two-phase flow simulations.

2.3. Models for particle response time

During the collapse process of a submerged granular column, either a high or low pore-pressure zone may occur inside the granular flow. The duration of the presence of the high or low pore pressure is an important factor affecting the collapse process. The drag force, which is modeled through the particle response time τ_p, may be responsible for the occurrence of the high or low pore-pressure zone as in the consolidation of soil (Das, 2013). When consolidating a soil, a high fluid pressure zone occurs inside the soil; the duration of the presence of the high pore pressure depends on the intrinsic permeability (k_p) (Das, 2013), and has an important influence on the consolidation. Because the particle response time (τ_p) can be related to the intrinsic permeability for dense two-phase flows (see Appendix B), we anticipate that computing τ_p accurately is crucial for liquid-solid two-phase flows.

Three models for particle response time are examined in this study, including a new model and two existing models (the model of Richardson and Zaki (1954) and the model of Engelund (1953)).

2.3.1. A model based on the sediment sedimentation in still water

The first model uses the particle response time computed by the following expression (Pitman and Le, 2005)

$$\tau_p = \frac{\rho_s}{\rho_f - \rho_s}\frac{w}{(1-c)^2 g}, \tag{18}$$

where w is the hindered velocity, or sedimentation velocity of many particles. The hindered velocity is smaller than the terminal velocity of a single particle, w_s, due to the influence of sediment concentration. Richardson and Zaki (1954) suggested

$$\frac{w}{w_s} = (1-c)^n, \tag{19}$$

where n is given by

$$n = \begin{cases} 4.65, & Re_s < 0.2 \\ 4.4Re_s^{-0.33}, & 0.2 \le Re_s < 1 \\ 4.4Re_s^{-0.1}, & 1 \le Re_s < 500 \\ 2.4, & 500 \le Re_s \end{cases} \tag{20}$$

with $Re_s = w_s d/\nu_f$. The terminal velocity of a single particle is computed by

$$w_s = \sqrt{\frac{4dg}{3C_d}\frac{\rho_s - \rho_f}{\rho_f}}, \tag{21}$$

where C_d is the drag coefficient for steady flows passing a small object (Engelund, 1953; Chien and Wan, 1999). For spheres, White (2000) suggested

$$C_d = \frac{24}{Re_p} + \frac{6}{1+\sqrt{Re_p}} + 0.4, \tag{22}$$

where $Re_p = |\mathbf{u}^f - \mathbf{u}^s|d/\nu_f$ (Eq. 3-255 in Ref. White (2000)). Combing Eqs. (18)-(22) yields

$$\tau_p = \frac{\rho_s}{\rho_f}\frac{d^2}{\nu_f}\frac{(1-c)^{n-2}}{18 + (4.5/(1+\sqrt{Re_p}) + 0.3)Re_p}. \tag{23}$$

The model based on Eq. (23) with Eq. (20) is referred to as "RZ model" in this study. Eq. (22) can be replaced by other formulas if the particle is not spherical. Eq. (19) is validated only for $c < 0.4$ (Yin and Koch, 2007). When the concentration c is so high that contact networks form among particles, w becomes zero; when this happens, Eq. (19) is not valid any more.

2.3.2. A model based on the pressure drop in steady flows through a homogenous porous media

The second model is based on the pressure drop in steady flows through a porous media. According the study of Engelund (1953), τ_p can be computed by

$$\tau_p = \frac{\rho_s d^2}{\rho_f \nu_f}\frac{1}{a_E c^2 + b_E Re_p}, \tag{24}$$

where a_E and b_E are the model parameters depending on the composition of the solid phase (see Appendix B). The parameter a_E varies from 780 to 5000 or more, and the parameter b_E varies from 1.8 to 3.6 or more (Yin and Koch, 2007; Burcharth and Andersen, 1995; Higuera et al., 2014). The parameter a_E is associated with k_p (see Appendix B). For $d \approx 2 \times 10^{-4}$ m, $k_p \approx 10^{-10} \sim 10^{-11}\text{m}^2$ (Das, 2013), which gives $a_E \approx 1.6 \times 10^3 \sim 1.6 \times 10^4$ for $c = 0.5$. In this study, $a_E = 5000$ and $b_E = 3.6$ are taken. The model based on Eq. (24) is referred to as Engelund model in this study.

2.3.3. A new model

Eq. (19) is validated only for $c < 0.4$ (Yin and Koch, 2007). To extend Eq. (19) to high concentration regions, Camenen (2005) modified Eq. (19) to

$$\frac{w}{w_s} = (1-c)^{n-1}[\max(1 - c/c_m, 0)]^{c_m}, \tag{25}$$

where c_m is the maximum concentration at which $w = 0$. In this study, $c_m = c_o$ is adopted because when $c \geq c_o$ contact networks can form in the granular material. Combining Eq. (18), Eq. (25), and Eqs. (20)-(22) gives

$$\tau_p = \frac{\rho_s}{\rho_f}\frac{d^2}{\nu_f}\frac{(1-c)^{n-3}[\max(1 - c/c_m, 0)]^{c_m}}{18 + (4.5/(1+\sqrt{Re_p}) + 0.3)Re_p}. \tag{26}$$

We stress that $c = c_m$ will lead to $\tau_p = 0$ and thus an infinite drag force. Physically, when the volume concentration is greater than some critical value, say c_r, Eq. (25) ceases to be valid and the

Engelund model should be used. To avoid unnaturally-large drag force between the two phases, we propose the following model for particle response time

$$\tau_p = \begin{cases} \frac{\rho_s}{\rho_f}\frac{d^2}{\nu_f}\frac{(1-c)^{n-3}[\max(1-c/c_m,0)]^{c_m}}{18+(4.5/(1+\sqrt{Re_p})+0.3)Re_p}, & \text{for } c < c_r \\ \frac{\rho_s d^2}{\rho_f \nu_f}\frac{1}{a_E c^2 + b_E Re_p}, & \text{for } c \geq c_r \end{cases} \tag{27}$$

where c_r is the concentration at the intercept point of Eq. (24) and Eq. (26). The transition from Eq. (26) to Eq. (24) is continuous at the intercept point where $c = c_r$. The concentration at the point joining the two models (c_r) is problem-dependent and can be found in principle by solving the following equation

$$\frac{(1-c_r)^{n-3}[\max(1-c_r/c_m,0)]^{c_m}}{18+(4.5/(1+\sqrt{Re_p})+0.3)Re_p} = \frac{1}{a_E c_r^2 + b_E Re_p}. \tag{28}$$

For given values of a_E and b_E, Eq. (28) implicitly defines c_r as a function of Re_p. We remark that it is not numerically efficient to solve Eq. (28) at every grid point for each time step. In Appendix C, we present a more computationally-efficient method to implement the new model in OpenFOAM.

2.3.4. Model comparison

The dimensionless particle response times, $\tau_p^* = \tau_p \nu_f \rho_f / d^2 \rho_s$, predicted by the aforementioned three models are presented in Fig. 1 as a function of either c or Re_p. When using the RZ and new models, $n = 4.65$ is adopted. The collapse of a submerged granular column involves high concentration flows where Re_p is very small (because the relative velocity is small in high concentration regions). Generally speaking, τ_p^* computed using these three models for low Re_p are not very sensitive to Re_p for a fixed c, but decrease with increasing with c for a fixed Re_p. When $c \to 0$, the new model reduces to the RZ model. For $0.064 < c < 0.54$, the RZ model gives the largest τ_p^*, but the Engelund model gives the smallest one when $c > 0.064$. When $c < 0.064$, the particle response time given by the Engelund model is much larger than those given by the other two models. For example, at $c = 0.01$, the Engelund model gives $\tau_p^* = 1.16$, but the other two models give $\tau_p^* = 0.045$. The particle response time τ_p^* computed by the new model drops dramatically from that by RZ model when c is close to 0.55.

2.4. Boundary conditions

In the simulation of the sediment phase, the no-slip boundary condition was imposed at the bed, but a slip boundary condition was imposed on the two lateral walls. In the simulation of the fluid phase, the wall-function method was imposed at the bed and on the two lateral walls. In view of the small size and the deep submergence of the granular column, the small vertical displacement of the fluid surface was ignored and a rigid lid approximation was adopted in the simulation.

2.5. Summary of model parameters

The RZ and Engelund models for particle response time have been implemented in the rheology-based two-phase model developed by Lee et al. (2016), which provides guidelines for choosing some of model parameters. The model parameters used in this study are summarized in Table 1, except for the parameters related to the low-Reynolds $k-\epsilon$ model. We treat the parameter b as a tuning parameter in this study; other parameters are treated as non-tuning parameters whose values are derived from the values reported in the literature. For the non-tuning parameters: $a = 0.11$ is suggested by Lee et al. (2016) for the sediment transport in the sheet flow condition; $I_o = 0.1$ is obtained numerically by Trulsson et al. (2012); Cassar et al. (2005) suggested $\eta_1 = 0.43$ and $\eta_2 = 0.82$ for glass beads; Boyer et al. (2011) suggested $c_c = 0.585$; $c_o = 0.55$ is the concentration for the loose packing granular column in the experiment of Rondon et al. (2011); Lee et al. (2015a) suggested $K = 10^8$ Pa and $\chi = 1.5$ for numerical stability consideration in modeling collapse of a

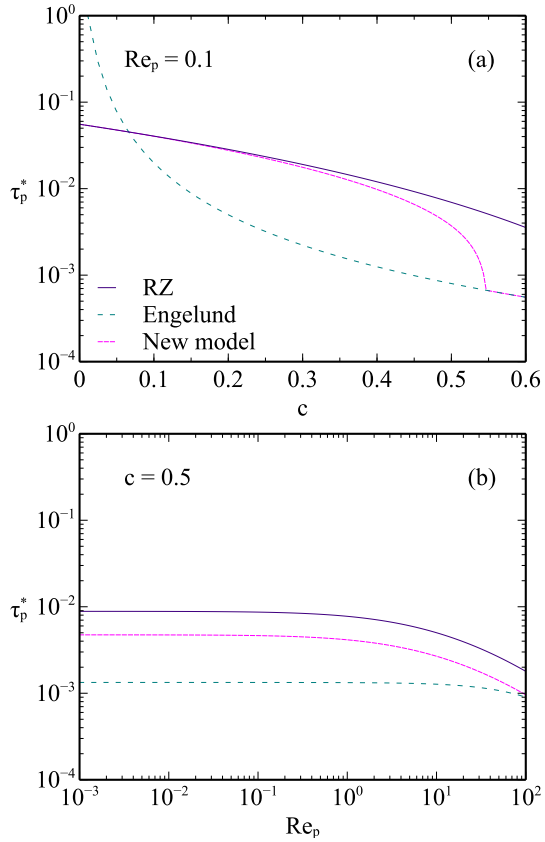

Fig. 1: Variations of dimensionless particle response time τ_p^* with c for $Re_p = 0.1$ [panel (a)] and with Re_p for $c = 0.5$ [panel (b)].

dry granular column; The values of $C_{\epsilon 3}$ and σ_c are the same as those used by Lee et al. (2016); the values of the two parameters are important for problems for sheet flows but not for the present problem. For the tuning parameter b, our numerical experiments found that the thickness of the flow front depended on the value of b and that $b = 2$ could give better results.

Table 1: Key model parameters used in this study.

a	b	I_o	η_1	η_2	c_o	c_c	c_{rcp}	K	χ	$C_{\epsilon 3}$	σ_c
0.11	2	0.1	0.43	0.82	0.55	0.585	0.64	10^8Pa	1.5	1	1

3. Numerical schemes

The equations in Section II are solved by using OpenFOAM, an open-source computational fluid dynamics (CFD) toolbox (Jasak, 2009). When using a two-phase model to simulate the collapse of a submerged granular column, a challenge is to ensure the numerical stability. When the concentration is high, the pressure of the solid phase [Eqs. (13) and (16)] is sensitive to small changes in concentration: a small fluctuation in concentration may lead to numerical instability. The numerical instability issue has been addressed by Lee et al. (2016), who incorporated into the PIMPLE scheme (OpenCFD, 2014) a perdition-correction scheme proposed by Lee et al. (2015a). The PIMPLE

scheme is a combination of the pressure implicit with splitting of operator scheme and the semi-implicit method for pressure-linked equations scheme. In the numerical scheme of Lee et al. (2015a), the discrete mass-balance equation for the sediment phase [Eq. (3)] becomes an advection-diffusion equation instead of an advection equation. The diffusion behavior helps subdue the fluctuation in concentration, and thus increases the numerical stability when the concentration is high.

4. Results and discussion

The two-phase model presented in the previous sections was used to simulate the collapse of a deeply-submerged granular column, as shown in Fig. 2. Three cases were simulated and the detailed conditions are listed in Table 2, which includes the properties of the fluid and sediment, the initial height H_i, and the initial width L_i. The new model for particle response time was used to compute τ_p for all the results presented in this section. The results obtained by the other two models will be discussed together with the sensitivity analysis in section 4.6.

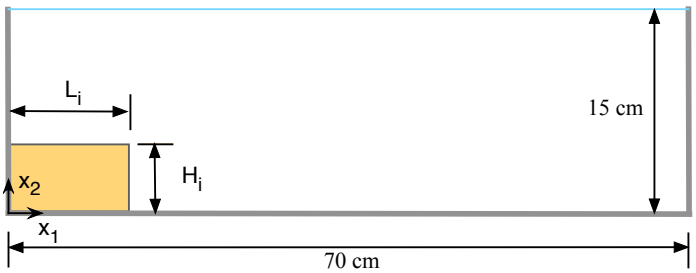

Fig. 2: Numerical set-up. Not drawn to scale.

Table 2: Collapse properties used in computations.

	ρ_f (kgm^{-3})	ν_f (cp)	ρ_s (kgm^{-3})	d (μm)	L_i (cm)	H_i (cm)	c_i
Case 1	1	10	2500	225	6	4.8	0.553
Case 2	1010	12	2500	225	6	4.8	0.553
Case 3	1010	12	2500	225	6	4.2	0.580

Case 1 simulates the collapse of a dry granular column. Cases 2 and 3 simulate the collapse of a granular column with an initially-loose packing and an initially-dense packing, respectively. These two cases have similar conditions except for the initial volume fraction c_i. Case 2 has an initial volume fraction $c_i = 0.553$, while Case 3 has an initial volume fraction $c_i = 0.580$. All three cases are used to verify the code and validate the present model: Case 1 is for the collapse of a dry granular column where the drag force is not important; Cases 2 and 3 are for the collapse of granular materials in a liquid where drag force is important. In particular, Case 1 is used to show that the present model can automatically provide a near-zero drag force for dry granular flows and thus reproduce the results given by the kinetic theory developed specifically for dry granular flows. Furthermore, comparing the results of Case 1 with those of Cases 2 and 3 can illustrate the role of drag force in the collapse of granular columns.

The convergence tests were performed using Case 2. A comparison of the flow-front location obtained by using $\Delta x = 2$ mm and $\Delta x = 1$ mm showed that the difference was less than 0.1%. Therefore, a grid size of $\Delta x = 1$ mm was used in all the simulations presented in this section. For this grid size, the relative variation of sediment mass was less than 10^{-5} during the entire collapse process. In all numerical simulations, Courant-Friedrichs-Lewy (CFL) number did not exceed 0.1.

In high concentration regions ($c > 0.55$), CFL number used in the simulations was smaller than 0.005 (Lee et al., 2016). Our simulations typically took a few hours for a physical time of 10 second using 8 threads on a workstation with two central processing units (Intel Xeon(R) CPU E5-2660 v2). If high performance computing (HPC) systems are available, the present model should be able to simulate large-scale problems without the need to modify the code[1].

In the experiment of Rondon et al. (2011), the collapse of the granular column was caused by suddenly lifting up the gate; however, the time series of the gate motion in the experiment were not provided in Rondon et al. (2011). The fast motion of the gate may result in a vertical fluid velocity on the interface between the granular material and the fluid. In the numerical simulations, the collapse of the granular column is caused by instantaneously removing the force holding the granular column in place. It is expected that this vertical velocity has effects only at the early stage of the collapse process. We have performed a simulation by imposing an initial upward velocity of 1 m/s in the fluid near the column. A comparison between the results obtained with and without this initial upward velocity has showed that the initial upward velocity has some influence at the initial stage of the collapse process ($t < 0.1$s), but the influence becomes insignificant at the later stage ($t > 1.32$ s). We remark that the intermittency found in the experiment of Rondon et al. (2011) does not occur in our simulated collapse process, regardless the presence of the vertical fluid velocity near the granular column.

4.1. Simulated collapse processes

Fig. 3 shows the simulated collapse process of the dry granular column. Good agreement can be observed between the results of the present two-phase model and those of Lee et al. (2015a), which was developed specifically for dry granular columns using an extension of granular kinetic theory. After the granular column collapses, the dry granular material spreads through avalanching and eventually stops. The collapse process is rapid and the final deposition profile is triangular-shaped. Because the initial concentration has insignificant effect on the collapse process of dry granular columns (Lee et al., 2015a), only the results for the loose packing case are presented here.

Fig. 4 shows the simulated collapse process for the granular column with an initially-loose packing (Case 2) and Fig. 5 for an initially- dense packing (Case 3). The experimental results (Rondon et al., 2011) are also included in these two figures for comparison. Comparing the collapse processes of the submerged columns (Figs. 4 and 5) with that of the dray column (Fig. 3) reveals that the collapse process, deposition profile and the duration for the submerged granular columns significantly differ from those for the dry granular column. Unlike the dry granular column, the collapse process of a submerged granular column is strongly affected by its initial packing. The collapse process of the loose-packing column (Case 2) is more rapid than that of the dense-packing column. The deposition profile for the loose packing is longer and thinner than that for the dense packing; however, the deposition profile for the dense packing is similar to that for the dry granular column. The simulated collapse processes for both Cases 2 and 3 are in general agreement with those observed in the experiment except for some minor discrepancies. The computed runout distance slightly exceeds the measurement for the dense packing case. The experiment video (Rondon et al., 2011) showed that the collapse of the dense-packing granular column was intermittent in the experiment (i.e., the granular material flowed and stopped alternatively), however, the computed collapse process is continuous.

The simulation overestimates the runout distance for the dense packing case, possibly because of the use of the wall function for the fluid phase. The wall-function method was proposed for clear water, and no wall-function applicable for a sediment-fluid mixture is available in the literature. Another possible reason is the particle response time used in the simulation. The hindered velocity changes sharply near $c = c_o$ (Camenen, 2005), so does the particle response time, which makes the

[1]We are in the process of implementing the model presented here on the TACC's Stampede2 system managed by XSEDE(Towns et al., 2014).

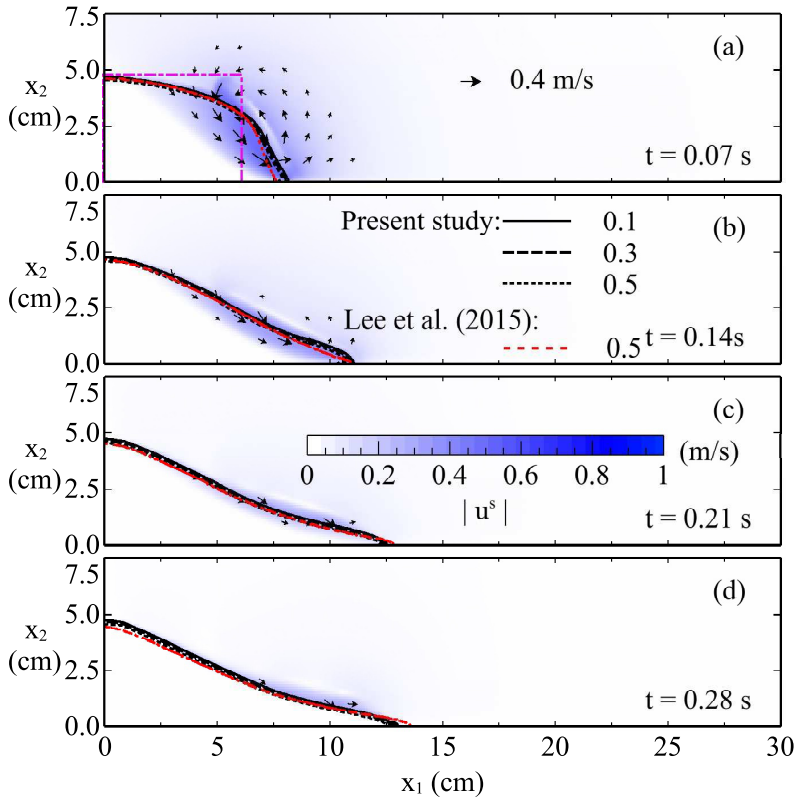

Fig. 3: Sequences of the collapsing process for Case 1. The lines represent contours of the computed concentrations, the color maps show the magnitude of the computed velocity of the solid phase. Velocity vectors for the solid phase are shown by arrows.

parameterization of particle response time near $c = c_o$ a challenge. Strictly speaking, the particle response time is also associated with the microscopic arrangements of particles (Yin and Koch, 2007) and affected by the presence of a wall as well (Chien and Wan, 1999). In our model for particle response time, the effects of both the presence of wall and the microscopic arrangements are not considered. We have also noted that the computed settling velocity near the flow front is slightly lower than that observed in the experiment video (Rondon et al., 2011).

Fig. 6 shows two examples of the computed velocity field of the sediment phase: one for the loose-packing case at $t = 0.66$ s and the other for the dense-packing case at $t = 3$ s. The loose-packing granular material spreads much faster than the dense-packing granular material does. Unlike in the loose-packing case where the whole body of the granular mass is moving, the region where the dense-packing granular mass has noticeable motion is confined to the lower corner of the frontal region.

We remark that the values of c_i used in the experiments were 0.55 for the loose packing and 0.6 for the dense packing; the latter is smaller than the value of c_i used in the simulation. Because $c_c = 0.585$, which is the maximum packing fraction of an homogeneously sheared assembly of frictional spheres (Boyer et al., 2011), the granular material with the initially-dense packing in the experiment will need to go through an internal adjustment under the shear action of the moving gate until the volume concentration reaches a value slightly smaller than c_c; before $c < c_c$ is reached, the granular material is not a frictional flow. Our choice of c_i means that the internal adjustment process is not simulated by the two-phase flow model.

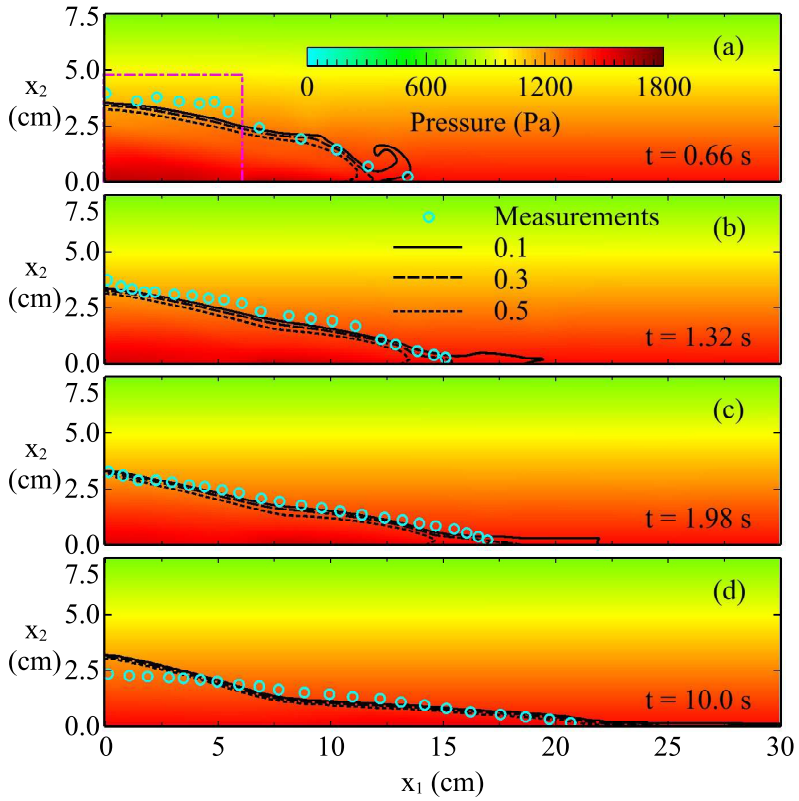

Fig. 4: Sequences of the collapsing process for Case 2. The lines represent contours of the computed concentrations and the color maps the computed pore pressure. The symbols were experimental data of of Rondon et al. (2011)

4.2. Vertical distribution of fluid pressure

To better show the deviation of the fluid pressure from the hydrostatic pressure, vertical distributions of the fluid pressure at four locations are presented in Fig. 7 for $t = 1.32$ s. As shown in Fig. 4, at $t = 1.32$ s the flow front defined by $c = 0.5$ reaches the location of x_1= 13 cm (the flow front defined by $c = 0.1$ reaches the location of x_1= 20 cm). At this time instant, the flow front define by $c = 0.5$ has not reached the location x_1=15 cm, but the flow front defined by $c = 0.1$ has passed this location. Referring to Fig. 7, the following conclusions can be drawn for the fluid pressure at these four locations: (1) the fluid pressure at x_1=15 cm is very close to hydrostatic; (2) an over-pressure at the bed can be clearly observed at x_1=5 cm, 7.5 cm and 10.0 cm; and (3) a sub-pressure at certain distance above the bed can be observed at x_1=7.5 cm or $x_1 = 10$ cm, but not at x_1=5.0 cm, which is too far from the flow front. For the collapse of dry granular materials, Roche et al. (2010) reported a sub-pressure at the bed where the flow front passed, which was followed by an over-pressure at the bed. We believe that the large viscosity of the fluid used in the experiment of Rondon et al. (2011) had prevented the sub-pressure from penetrating down to the bed.

4.3. Contractancy and dilatancy

Shearing and volumetric strains are coupled during the deformation of a granular material. It is well known in soil mechanics that shear deformations of sand often are accompanied by changes in volume: loose sand has a tendency to contract to a smaller volume, but densely-packed sand cannot deform without expanding (Campbell, 2006). The former phenomenon is called contractancy and the latter dilatancy. Accompanying with the change in volume of sand is a change in shear stress: loose sand shows a gradual increase in shear stress, while densely-packed sand shows a decrease in

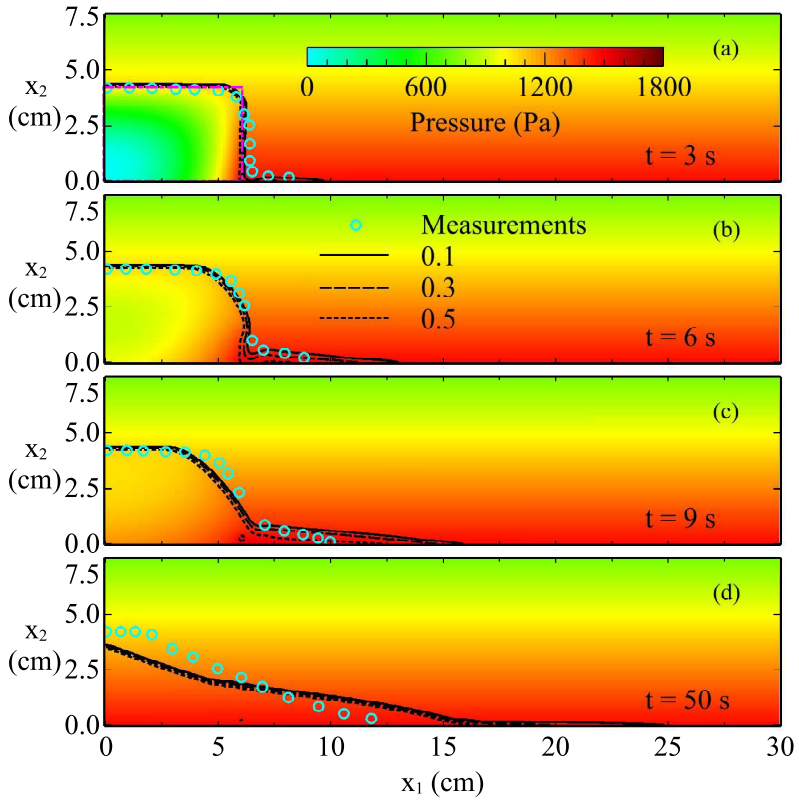

Fig. 5: Same as Fig. 4 but for Case 3.

shear stress. Both the loose and densely-packed granular materials have a tendency to ultimately attain a critical-state shear stress.

We have chosen to use the temporal variations of the maximum concentrations in both the initially-loose and initially-dense packing conditions to show the contractancy and dilatancy behaviors. We have tried to show contractancy and dilatancy behaviors using the temporal variation of the total volume or mean concentration, but the the suspension of the granular material makes it difficult to define a clear interface between the fluid and granular material; any interface defined based on a specified concentration will show a loss of granular mass. A decrease/increase of the maximum concentration indicates a dilatancy/contractancy behavior. It can be seen from Fig. 8 that the granular material with an initially-loose packing undergoes a contracting process (contractancy) whiles the granular material with an initally-dense packing goes through a dilatant process (dilatancy). Our results shows that Rondon et al. (2011)'s conjecture about the dilatancy/contractancy behavior is correct.

Because increasing/decreasing the volume concentration c increases/decreases the pressure of the sediment phase p_s, the contractancy/dilatancy found in both the experiment and simulation is related to the low/high pressure of the sediment phase p_s in the loosely/densely packing column. Therefore, how to compute p_s is important for simulating the collapse of submerged granular columns. In this study, Eqs. (13) and (16) are used to compute p_s. Eq. (13) reflects the elastic effect and Eq. (16) reflects the rheological characteristic related to D^s. Eq. (13) says that a lower c_i yields a lower p_{se}; if the force due to p_{se} is not large enough to support the weight of solid phase, the lower p_{se} will induce contractancy. On the other hand, a higher c_i will induce dilatancy. Eq. (16) implies that a lower/higher c_i yields a lower/higher for a certain D^s. However, the above intuitive explanation based on Eqs. (13) and (16) does not consider the complex behavior of a granular flow

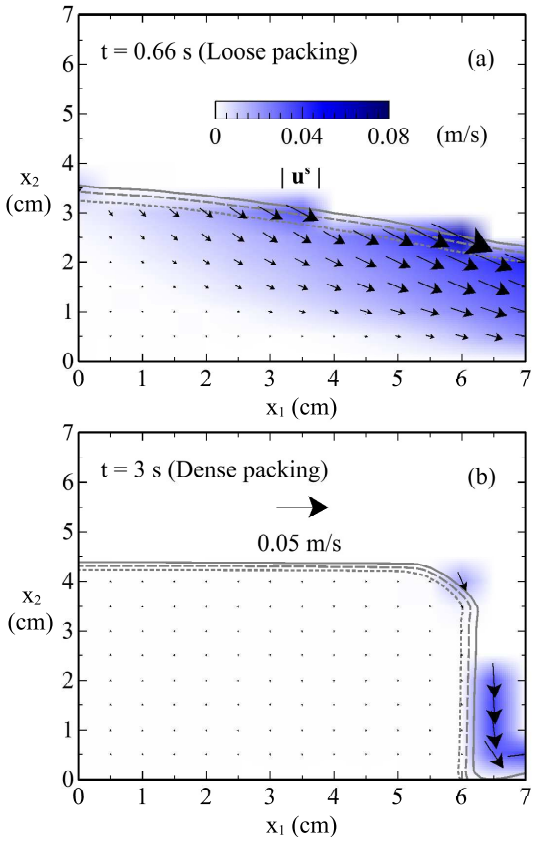

Fig. 6: Velocity field of the solid phase ($\mathbf{u}^s$) computed with the new model for the loose-packing case (a) and the dense-packing case (b). The arrows show the velocity vectors for the solid phase with the color maps showing the magnitudes of the computed velocity of the solid phase in the background.

near its static state due to the rearrangement of particles. For the dense-packing case, it can be observed that the volume of the granular material slightly expands and c_{max} decreases from 0.58 to 0.565 within $t < 0.5$ s; this is due mainly to the large elastic energy in the granular material. To check the influence of the expansion on the collapse process, we have performed simulations using $c_i = 0.565 - 0.58$ and found that the results are not sensitive to changes in c_i within this range.

4.4. General buoyancy and drag force

General buoyancy and drag are two important forces influencing the collapse process. General buoyancy is directly related to the the pressure of the fluid phase (i.e., pore pressure) and the drag force is directly related to the relative motion between the two phases.

Referring to Fig. 4, a high pore-pressure zone can be observed inside the granular flow with an initially-loose packing, and the high pore-pressure dissipates with the spreading of the granular material. However, a low pore-pressure zone can be observed inside the granular flow with an initially-dense packing as shown in Fig. 5, and both the zone size and magnitude of the low pore pressure decrease gradually with the spreading of the granular material.

The gradient in the pore-pressure field will produce a pressure force on the sediment phase, called general buoyancy. The dynamic components of the general buoyancy, $-\nabla p_f^d$, where $p_f^d = p_f - \rho_f g x_2$ with $g = |\mathbf{g}|$, are shown in Fig. 9 for Cases 2 and 3 (the rest part of the general buoyancy is always the constant $\rho_f g$). For the loose packing case, the general buoyancy points outward, which helps

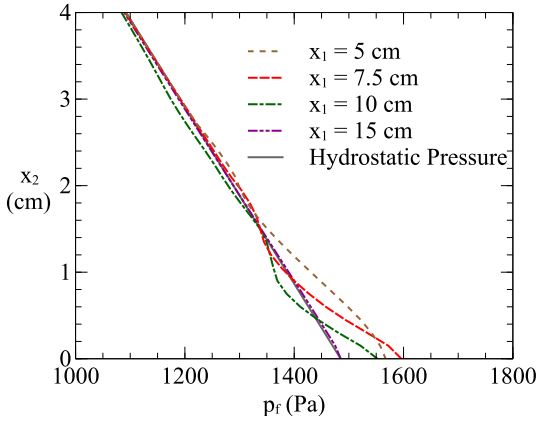

Fig. 7: Vertical distributions of fluid pressure at four locations (x_1 = 5, 7.5, 10, and 15 cm) at t = 1.32 s for Case 2.

to destabilize the granular mass; for the dense packing, the general buoyancy points inward, which helps to stabilize the granular mass.

When contractancy/dilatancy occurs, the amount of fluid inside the granular material decreases/ increases, resulting in a relative motion between the sediment and fluid phases near the surface of the granular mass. Fig. 10 shows the relative velocity between the two phases for both the loose and dense packing cases. Although the relative velocities inside the granular material are very small, the drag force can still be comparable to the dynamic component of the general buoyancy when the particle response time τ_p is small. The drag forces for Cases 2 and 3 are presented in Fig. 11. For the loose packing case, the drag force points nearly vertically upward, which helps to destabilize the granular mass; for the dense packing case, however, the drag force points inward, which helps to stabilize the granular mass.

It can be seen from Figs. 9 and 11 that the general buoyancy and the drag force have similar magnitudes and patterns except near the surface of the moving granular mass; both the general buoyancy and drag force turn to destabilize the loosely-packed granular mass, but stabilize the densely-packed granular mass.

4.5. Duration of the collapse process

The durations of the collapse process for Cases 2 and 3 are much longer than that for the dry column (Case 1). Further comparing Cases 2 and 3 shows that the duration for Case 3 is one order-of-magnitude longer than that for Case 2. For a deeply-submerged granular column, the drag force and the general buoyancy [the third term on the right-hand-side of Eq. (4)] both influence the collapse process: the drag force dissipates the kinetic energy in the granular martial, while the general buoyancy reduces the gravitational effect. For the loose-packing case (Case 2), the high pore-pressure zone developed inside the granular material leads to an outward general buoyancy, and the fluid flowing out near the surface yields another outward drag force acting on the solid phase; both forces tend to further destabilize the loosely-packed granular material, leading to a rapid collapse process. For the dense-packing case (Case 3), however, the low-pore pressure zone developed inside the granular material yields an inward general buoyancy, and the inward flow near the surface also yield an inward drag force; both forces tend to stabilize the densely-packed granular material, leading to a slow collapse process.

4.6. Sensitivity analysis

A sensitivity analysis has been performed to examine how sensitive the collapse process is to the key model parameters, including the particle response times obtained using three models. The ranges of these parameters used in the sensitivity analysis are summarized in Table 3 and Table 4.

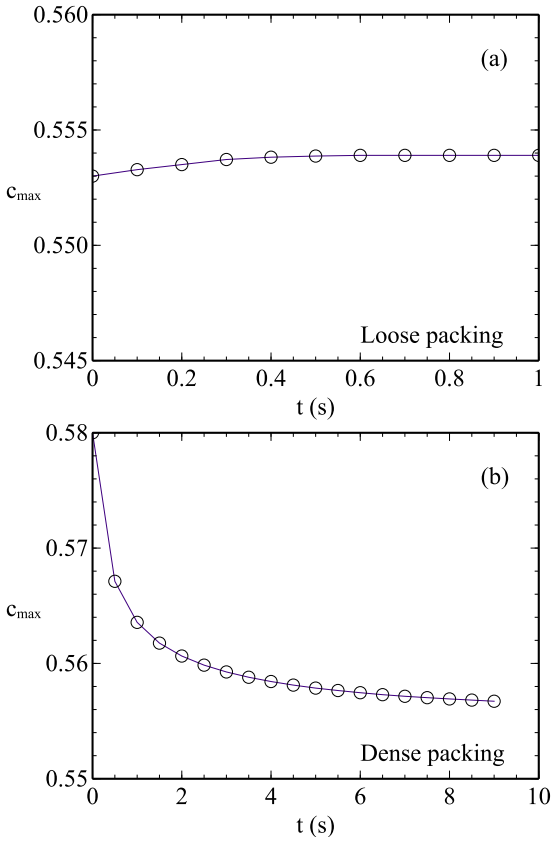

Fig. 8: Change of c_{max} with time for the loose-packing case (a) and for the dense-packing case (b).

For the loose-packing case, the corresponding ranges of H and L at $t = 0.66$ s are listed in Table 3. For the dense packing case, however, only the ranges of L at $t = 9$ s are listed in Table 4 because the values of H for these cases are the same as those of H_i except for the case where the Engelund model is used to compute τ_p. The ranges of the parameters tested in the sensitivity analysis are based on the following considerations:

1. I_o (Trulsson et al., 2012; Pouliquen et al., 2006), $1/\sigma_c$ (Lee et al., 2015b; Hsu et al., 2003), and $C_{\epsilon 3}$ (Lee et al., 2016) cover the values reported in literature.
2. The ranges of K, χ, and c_{rcp} are identical to those used in Lee et al. (2015a) for simulating the collapse of a dry granular column.
3. a varies from 0.01 to 1 in the literature (Trulsson et al., 2012; Chiodi et al., 2014; Lee et al., 2016), we take $a = 0 - 0.5$ for numerical stability considerations.
4. The range of b reported in the literature varies from 0.75 to 1 (Boyer et al., 2011; Revil-Baudard and Chauchat, 2013), but $b = 1 - 3$ was used in this sensitivity analysis because numerical instability occurred when $b < 1$.
5. We chose the ranges of c_c and η_1 to cover the values reported in the literature (Cassar et al., 2005; Simons and Albertson, 1960; Nielsen, 1992; Hanes and Inman, 1985; Sperry and Peirce, 1995), i.e., $c_c = 0.585 - 0.615$ and $\eta_1 = 0.43 - 0.73$ which cover both glass beads and sand (Boyer et al., 2011; Bear, 1972).
6. Since η_2 must be larger than or equal to η_1, η_2=0.43-0.82 were adopted in the analysis.

The three models (RZ, Engelund, and the new model) for particle response time, τ_p, were also compared in the sensitivity analysis.

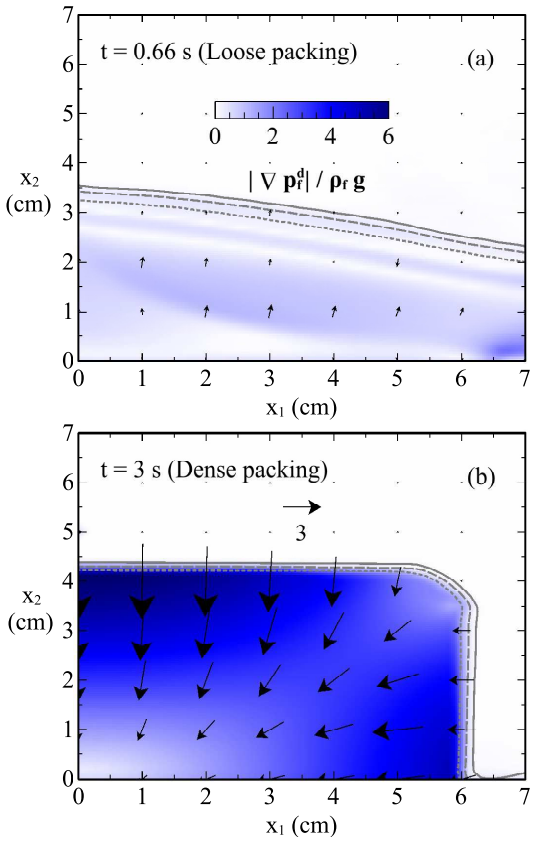

Fig. 9: The general buoyancy computed by the new model for the loose-packing case (a) and the dense-packing case (b). The arrows show the gradient with the color map showing in the background the magnitude of the dynamic component of the general buoyancy.

It can be seen from Table 3 that the parameters K and χ in Eq. (13) are the most important parameters affecting the collapse of a loose-packing granular column. The other two parameters b and c_c in Eq. (16) are also important. These four parameters (K, χ, b, and c_c) are needed to compute the pressure of the solid phase, and thus the dilatancy or contractancy behavior relies on these four parameters in addition to the initial packing specified by c_i. Furthermore, these four parameters indirectly influence the friction in the solid phase. The parameters η_1, η_2, and I_o in Eq. (14) and τ_p can also affect the collapse process, but to a lesser extent. It is a surprise to note that both σ_c and $C_{\epsilon 3}$ have insignificant effects on the collapse process. We remark that σ_c is associated with the turbulent dispersion of the sediment phase and $C_{\epsilon 3}$ the turbulence modulation due to the presence of the sediment phase. Even though the turbulence modulation seems to have insignificant influence on the collapse process of a loose-packing granular column studied here, for other types of two-phase flow problems, such as sediment transport driven by turbulent flows, σ_c and $C_{\epsilon 3}$ are important.

For the collapse of a dense-packing granular column, Table 4 shows that K, χ, b, c_c, η_1, and η_2 are equally important. However, the particle response time τ_p becomes the most important parameter for the dense-packing case. To show this, we compare the collapse processes simulated by using the RZ (Fig. A.1) model, the Engelund (Fig. A.2) model, and the new model (Fig. 5). The collapse process given by the RZ model is the most rapid one because the RZ model gives the largest τ_p (or the smallest drag force).Comparing the computed results obtained using the Engelund model and

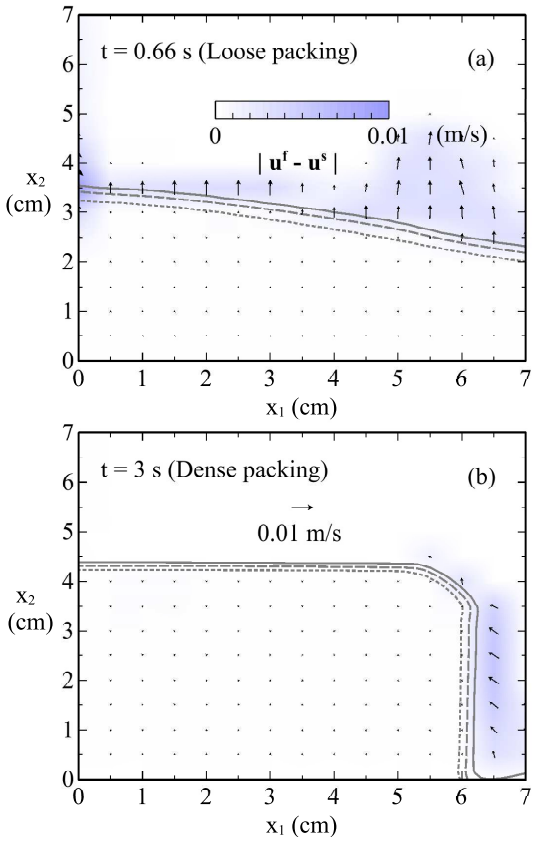

Fig. 10: The relative velocity fields ($\mathbf{u}^f - \mathbf{u}^s$) for the loose packing case (a) and the dense-packing case (b). The arrows show the velocity vectors with the color map showing the magnitude of the relative velocity in the background.

the new model, the new model shows a quicker deposition near flow front ($x > 10$ cm) when $t = 9$ s; this is because the new model gives a smaller τ_p when $c < 0.54$. A good agreement between the experimental results and the numerical results obtained by the new model can be observed in Fig. 5, which proves our hypothesis that modifying the RZ model for high concentration and using a limiter for even higher concentration is important for correctly modeling the drag force in granular flows with an initially-dense packing.

As mentioned in Section 4.1, a high/low pore-pressure zone occurs in the granular flow with an initially dense/loose packing, and it strongly influences the collapse process. Fig. 12 shows the variations of the minimum value of p_f^d for the dense-packing case (p_{min}^d) and the maximum value for the loose-packing case (p_{max}^d). It can be seen that p_{min}^d for the dense-packing case is one order-of-magnitude larger than p_{max}^d for the loose-packing case. The model for τ_p has a significant effect on p_f^d for the dense-packing case, but has an insignificant effect for the loose-packing case. One explanation is that the dilatancy in dense-packing case generates a relative velocity much larger than that generated by the contractancy in the loose-packing case (see Fig. 8), which makes the drag force in the dense-packing granular material more much sensitive to the model for τ_p.

5. Conclusions

Using a continuum two-phase flow approach, this study introduced a new model for particle response time to simulate the collapse of a granular column deeply submerged in a fluid. For both

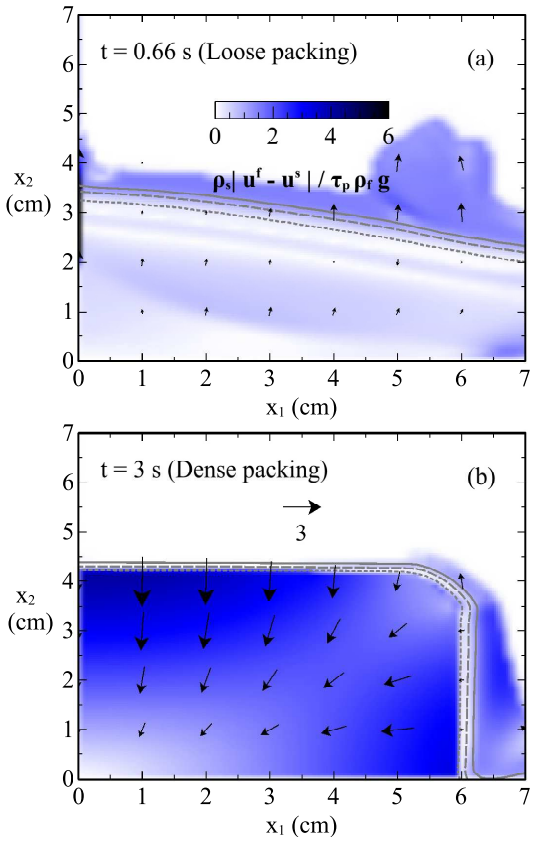

Fig. 11: The drag forces acting on the sediment phase (computed with the new model) for the loose- packing case (a) and for the dense-packing case (b). The arrows show the gradient with the color maps showing in the background the magnitudes of the drag force.

initially loose and dense packing conditions, the two-phase flow model with the new model for particle response time was able to simulate the collapse processes in general agreement with existing laboratory observations for both loose and dense packing conditions.

The numerical results showed that contractancy and dilatancy occur, respectively, for loose packing and dense packing during the collapse process, validating Rondon et al. (2011)'s conjecture about how initial volume fraction affect collapsing processes.

The general buoyancy and drag force were found to have similar directions and their magnitudes. The contractancy induced a high pore-pressure zone inside the loose-packing granular material, which generated an outward force on the sediment near the surface and helped to destabilize the granular mass. The dilatancy induced a low pore-pressure zone inside the dense-packing granular material, which produced an inward force on the sediment near the surface and helped to stabilize the granular mass.

A sensitivity analysis was performed by varying key model parameters involved in the computation of the sediment-phase pressure because the contractancy or dilatancy of the granular material is related to the sediment-phase pressure. Large relative velocities between the sediment and fluid phases were found near the surface of the moving granular mass for the dense-packing condition. It was concluded that the collapse process of a densely-packed granular column was more sensitive to particle response time than that of a loosely-packed granular column

Possible further research directions in two-phase modeling of submarine granular flows include:

Table 3: Summary of sensitivity analysis on height H and width L for the loose packing column at $t = 0.66$ s. The base values correspond to $H = 3.30$ cm and $L = 11.1$ cm.

Varying parameter	Varying ranges	H (cm)	L (cm)
a	$0 \rightarrow 0.5$	$3.4 \rightarrow 3.25$	$10.5 \rightarrow 11.3$
b	$1 \rightarrow 3$	$2.83 \rightarrow 3.5$	$14.7 \rightarrow 9.4$
c_c	$0.585 \rightarrow 0.615$	$3.30 \rightarrow 2.90$	$11.1 \rightarrow 14.7$
I_o	$0 \rightarrow 0.3$	$3.43 \rightarrow 3.21$	$10.0 \rightarrow 11.8$
η_1	$0.43 \rightarrow 0.73$	$3.30 \rightarrow 3.61$	$11.1 \rightarrow 10.1$
η_2	$0.43 \rightarrow 0.82$	$3.18 \rightarrow 3.30$	$12.2 \rightarrow 11.1$
$1/\sigma_c$	$0 \rightarrow 2$	$3.27 \rightarrow 3.27)$	$11.3 \rightarrow 11.3$
$C_{\epsilon 3}$	$1 \rightarrow 1.6$	$3.30 \rightarrow 3.27$	$11.1 \rightarrow 11.3$
K	$10^5 \rightarrow 10^9$	$2.45 \rightarrow 4.72$	$13.1 \rightarrow 6.2$
χ	$1 \rightarrow 3.5$	$4.72 \rightarrow 2.45$	$6.0 \rightarrow 13.1$
c_{rcp}	$0.62 \rightarrow 0.64$	$3.75 \rightarrow 3.30$	$10.2 \rightarrow 11.1$
τ_p	RZ, Engelund, new	$2.57, 3.24, 3.30$	$13.8, 11.5, 11.1$
c_i	$0.552 \rightarrow 0.554$	$2.63 \rightarrow 4.36$	$13.0 \rightarrow 8.7$

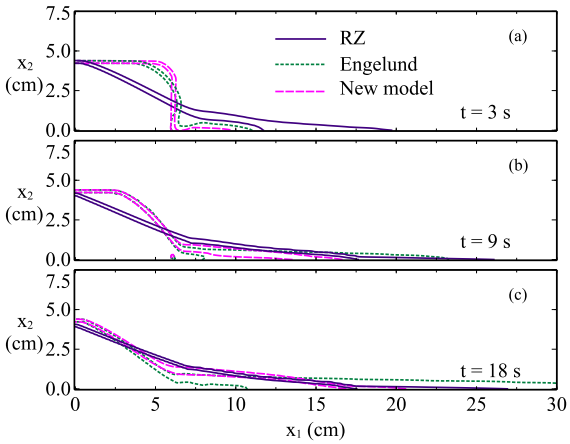

Fig. 12: p^d_{max} varying with time for the loose packing (a) and p^d_{min} for the dense packing (b).

(i) plastic effect in the computation of the pressure of the solid phase; (ii) near-wall correction to the sedimentation velocity; (iii) effect of sediment phase on the wall function for modeling fluid phase.

Acknowledgements

The material is based on work supported by the Ministry of Science and Technology, Taiwan (MOST 105-2218-E-032-001-) and the National Science Foundation under grant No. CBET-1706938. Part of this work used the Extreme Science and Engineering Discovery Environment (XSEDE) through a Startup Allocation (OCE170015). Any opinions, findings, and conclusions or recommendations expressed in this material are those of the author(s) and do not necessarily reflect the views of the National Science Foundation. This is SOEST contribution No. 10286.

Table 4: Summary of sensitivity analysis on L for the dense packing column at $t = 9$ s. The base values correspond to $L = 13.5$ cm.

Varying parameter	Varying ranges	L (cm)
a	$0 \to 0.5$	$13.2 \to 13.5$
b	$1 \to 3$	$17.1 \to 11.8$
c_c	$0.585 \to 0.615$	$13.5 \to 15.2$
I_o	$0 \to 0.3$	$13.1 \to 13.7$
η_1	$0.43 \to 0.73$	$13.5 \to 10.6$
η_2	$0.43 \to 0.82$	$12.9 \to 14.3$
$1/\sigma_c$	$0 \to 2$	$13.3 \to 13.7$
$C_{\epsilon 3}$	$1 \to 1.6$	$13.5 \to 13.7$
K	$10^5 \to 10^9$	$14, 12.2, 16.8$
χ	$1 \to 3.5$	$16.3, 12.2, 17.0$
c_{rcp}	$0.62 \to 0.64$	$14.4 \to 13.5$
τ_p	RZ, Engelund, new	$13.5, 8.1, 13.5$
c_i	$0.565 \to 0.58$	$14.1 \to 13.5$

Appendix A. The simulated collapse processes of granular columns by using particle response models of Richardson and Zaki (1954) and Engelund (1953)

Figs. A.1 shows the collapse processes of an initially-dense packing column simulated by using the model of Richardson and Zaki (1954), referred to as RZ in the figure. A.2 shows the collapse processes of an initially-dense packing column simulated by using the model of Engelund (1953), referred to as Engelund in the figure. The measured results of Rondon et al. (2011) and the results obtained by using the new model are also superposed in these two figures for comparison. As it can be seen from these two figures, the agreement between the measurement and the numerical results obtained by RZ and Engelund models is not satisfactory: the collapse process simulated by the RZ model is too fast; granular suspension simulated by Engelund model is too strong (see the two lines indicating the concentrations of $c = 0.1$ and $c = 0.5$).

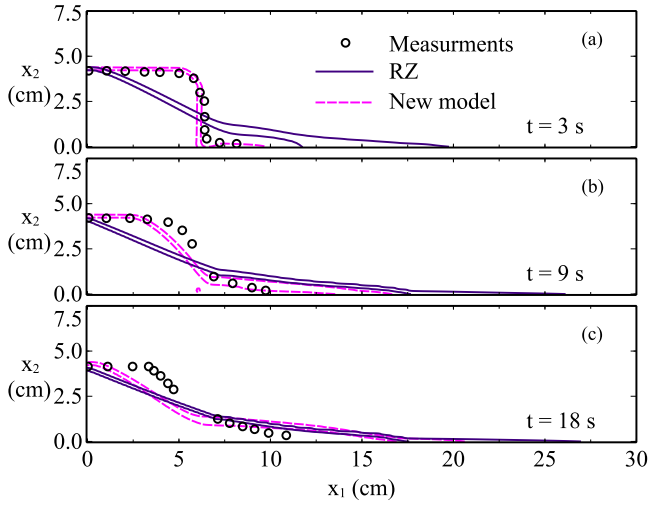

Fig. A.1: The contours of the simulated concentrations of $c = 0.1$ and 0.5 for the initially-dense packing column using the RZ model. The concentration c decreases outward. The symbols were experimental data of Rondon et al. (2011)

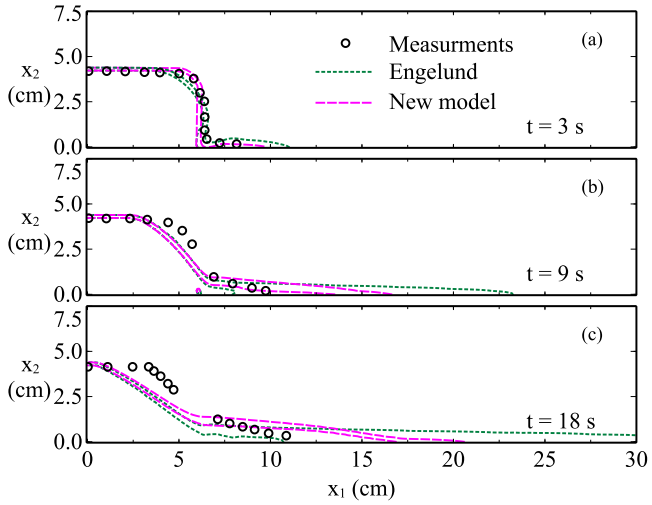

Fig. A.2: Same as Fig. A.1 but for the Engelund model.

The collapse processes of an initially-loose packing column simulated by using the RZ and Engelund models are presented in in Figs. A.3 and A.4, respectively. The measured results of Rondon et al. (2011) and the results obtained by using the new model are also superposed in these two figures for comparison. The agreement between the measurement and the numerical results obtained by RZ model is reasonably well except that the RZ model slightly over-predict the height in the region close to $x = 0$. The agreement between the measurement and the numerical results obtained by Engelund model is less satisfactory: the model over predicts the runout distance significantly.

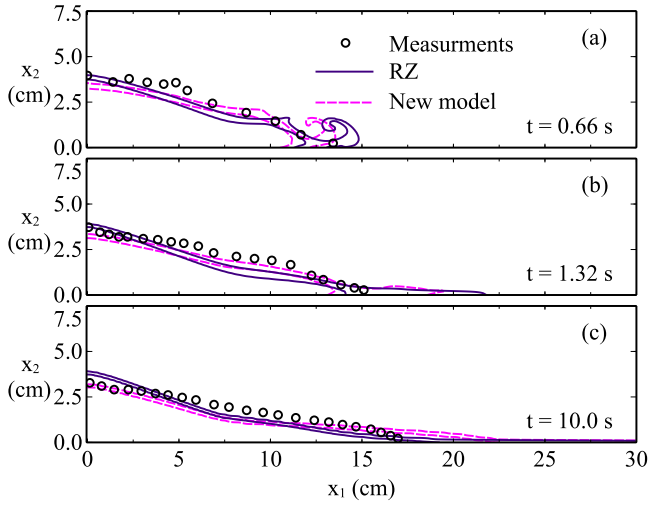

Fig. A.3: The contours of the simulated concentrations of $c = 0.1$ and 0.5 for the initially-loose packing column using the RZ model. The concentration c decreases outward. The symbols were experimental data of Rondon et al. (2011)

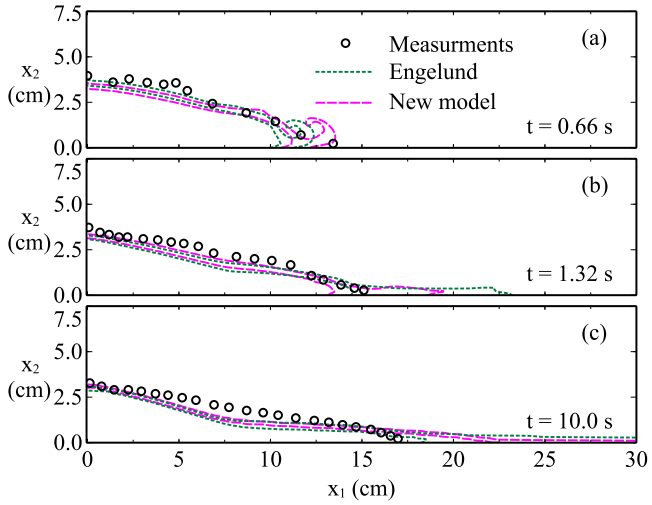

Fig. A.4: Same as Fig. A.3 but for the Engelund model.

Appendix B. A relationship between particle response time and permeability

For a one-dimensional problem of a steady flow through porous media, the terms containing the stresses of fluid phase disappear, and Eq. (2) reduces to

$$-\frac{\partial p_f}{\partial x_1} = \frac{c\rho_s u_1^f}{(1-c)\tau_p}, \tag{B.1}$$

where the coordinate x_1 points in the direction of the flow. For this problem, Forchheimer Bear (1972) suggested

$$-\frac{\partial p_f}{\partial x_1} = a_F \rho_f (1-c) u_1^f + b_F \rho_f (1-c)^2 u_1^{f2}, \tag{B.2}$$

where a_F and b_F are two model parameters. Engelund (1953) suggested

$$a_F = \frac{a_E c^3 \nu_f}{(1-c)^2 d^2}, \tag{B.3}$$

and

$$b_F = \frac{b_E c}{g(1-c)^3 d}, \tag{B.4}$$

where a_E and b_E are two model parameters. After comparing Eqs. (B.1) and (B.2) and using Eqs. (B.3) and (B.4), one can obtain

$$\tau_p = \frac{\rho_s d^2}{\rho_f \nu_f} \frac{1}{a_E c^2 + b_E Re_p}, \tag{B.5}$$

According to Darcys law for seepage (Bear, 1972), the pressure gradient is

$$-\frac{\partial p_f}{\partial x_1} = \frac{\rho_f \nu_f (1-c) u_1^f}{k_p}, \tag{B.6}$$

where k_p is the permeability.

When the flow is very slow, Eqs. (B.2), (B.3) and (B.6) suggest that

$$a_E = \frac{d^2}{k_p (1-c)^2}, \tag{B.7}$$

which means that the particle response time can be related to the permeability.

Appendix C. Implementation of the new model for τ_p in OpenFOAM

For the problem studied here, we have used $a_E = 5000$ and $b_E = 3.6$ and the dependence of c_r on Re_p is weak. The curve $c_r(Re_p)$ is shown in Fig.C.1 for $0.1 < Re_p < 10$ (the upper limit of Re_p is determined by assuming $Re_p = Re_s$; for the sand diameter used in our numerical simulations, $Re_s \sim 7$). We remark that whenever there are two solutions for c_r, the one with the larger concentration should be taken. There are two solutions when $Re_p < 8.2$, but only one solution for $Re_p > 8.1$. In any case, the value of c_r should be the one given by the upper curve, which is not very sensitive to Re_p for the problem studied here. Referring to Fig.C.1, when $c > c_r$, the Engeland

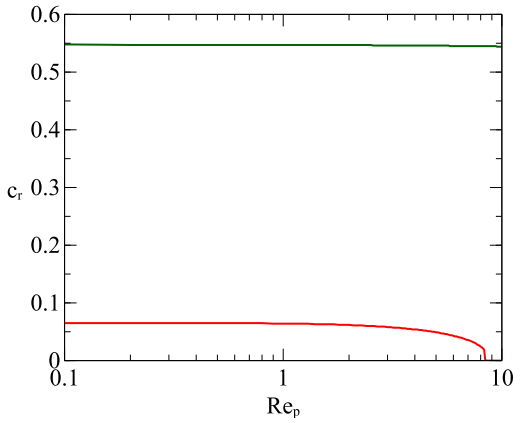

Fig. C.1: c_r as a function of Re_p for $a_E = 5000$ and $b_E = 3.6$.

model should be used to calculate τ_p; when $0.5 < c < c_r$, the RE model should be used to calculate τ_p; when $c < 0.5$ the RE model should be used. Therefore, in consideration of the computational efficiency and in view of Fig. C.1, the model described by Eq. (27) can be numerically implemented in OpenFOAM by using following continuous piecewise function,

$$\tau_p = \begin{cases} \frac{\rho_s}{\rho_f}\frac{d^2}{\nu_f}\frac{(1-c)^{n-3}[\max(1-c/c_m,0)]^{cm}}{18+(4.5/(1+\sqrt{Re_p})+0.3)Re_p}, & \text{for } c < 0.5 \\ \max\left(\frac{\rho_s}{\rho_f}\frac{d^2}{\nu_f}\frac{(1-c)^{n-3}[\max(1-c/c_m,0)]^{cm}}{18+(4.5/(1+\sqrt{Re_p})+0.3)Re_p}, \frac{\rho_s d^2}{\rho_f \nu_f}\frac{1}{a_E c^2 + b_E Re_p}\right), & \text{for } c \geq 0.5 \end{cases} \tag{C.1}$$

which can avoid solving the equation for c_r at every grid point for each time step, and thus is more computationally efficient.

References

D. G. Masson, C. B. Harbitz, R. B. Wynn, G. Pedersen, F. Løvholt, Submarine landslides: processes, triggers and hazard prediction., Philos. Trans. A. Math. Phys. Eng. Sci. 364 (1845) (2006) 2009–2039, ISSN 1364-503X, doi:\let\@tempa\bibinfo@X@doi10.1098/rsta.2006.1810.

S.-K. Hsu, J. Kuo, C.-L. Lo, C.-H. Tsai, W.-B. Doo, C.-Y. Ku, J.-C. Sibuet, Turbidity Currents, Submarine Landslides and the 2006 Pingtung Earthquake off SW Taiwan, Terr. Atmos. Ocean. Sci. 19 (6) (2008) 767, ISSN 10170839, doi:\let\@tempa\bibinfo@X@doi10.3319/TAO.2008.19.6.767(PT)1.

E. Lajeunesse, A. Mangeney-Castelnau, J. P. Vilotte, Spreading of a granular mass on a horizontal plane, Phys. Fluids 16 (7) (2004) 2371–2381, doi:\let\@tempa\bibinfo@X@doi10.1063/1.1736611.

E. Lajeunesse, J. B. Monnier, G. M. Homsy, Granular slumping on a horizontal surface, Phys. Fluids 17 (10) (2005) 103302, doi:\let\@tempa\bibinfo@X@doi10.1063/1.2087687.

G. Lube, H. E. Huppert, R. S. J. Sparks, M. A. Hallworth, G. Flows, T. Physics, W. Road, Axisymmetric collapses of granular columns, J. Fluid Mech. 508 (1) (2004) 175–199, doi:\let\@tempa\bibinfo@X@doi10.1017/S0022112004009036.

G. Lube, H. E. Huppert, R. S. J. Sparks, A. Freundt, Static and flowing regions in granular collapses down channels, Phys. Fluids 19 (2007) 43301.

G. Lube, H. E. Huppert, R. S. Sparks, A. Freundt, Collapses of two-dimensional granular columns, Phys. Rev. E 72 (4) (2005) 041301.

R. Zenit, Computer simulations of the collapse of a granular column, Phys. Fluids 17 (3) (2005) 031703, doi:\let\@tempa\bibinfo@X@doi10.1063/1.1862240.

L. Girolami, V. Hergault, G. Vinay, A. Wachs, A three-dimensional discrete-grain model for the simulation of dam-break rectangular collapses: comparison between numerical results and experiments, Granul. Matter 14 (3) (2012) 381–392, doi:\let\@tempa\bibinfo@X@doi10.1007/s10035-012-0342-3.

L. Lacaze, J. C. Phillips, R. R. Kerswell, Planar collapse of a granular column: Experiments and discrete element simulations, Phys. Fluids 20 (6) (2008) 063302, ISSN 1070-6631, doi:\let\@tempa\bibinfo@X@doi10.1063/1.2929375.

P. G. Rognon, I. Einav, C. Gay, P. G. Rognon, I. Einav, C. Gay, Flowing resistance and dilatancy of dense suspensions : lubrication and repulsion, J. Fluid Mech. 689 (2011) 75–96, doi:\let\@tempa\bibinfo@X@doi10.1017/jfm.2011.397.

F. Boyer, O. Pouliquen, E. Guazzelli, Dense suspensions in rotating-rod flows: normal stresses and particle migration, J. Fluid Mech. 686 (2011) 5–25, doi:\let\@tempa\bibinfo@X@doi10.1017/jfm.2011.27.

C. Cassar, M. Nicolas, O. Pouliquen, Submarine granular flows down inclined planes, Phys. Fluids 17 (10) (2005) 103301, ISSN 10706631, doi:\let\@tempa\bibinfo@X@doi10.1063/1.2069864.

M. Trulsson, B. Andreotti, P. Claudin, Transition from the Viscous to Inertial Regime in Dense Suspensions, Phys. Rev. Lett. 109 (11) (2012) 118305, ISSN 0031-9007, doi:\let\@tempa\bibinfo@X@doi10.1103/PhysRevLett.109.118305.

R. M. Iverson, M. Reid, N. Iverson, R. LaHusen, M. Logan, J. Mann, D. Brien, Acute sensitivity of landslide rates to initial soil porosity, Science 290 (20) (2000) 513–516.

P.-Y. Lagrée, L. Staron, S. Popinet, The granular column collapse as a continuum: validity of a two-dimensional NavierStokes model with a μ (i)-rheology, J. Fluid Mech. 686 (1) (2011) 378–408.

I. R. Ionescu, A. Mangeney, F. Bouchut, O. Roche, Viscoplastic modelling of granular column collapse with pressure dependent rheology, J. Nonnewton. Fluid Mech. 219 (2015) 1–18, ISSN 03770257, doi:\let\@tempa\bibinfo@X@doi10.1016/j.jnnfm.2015.02.006.

C.-H. Lee, Z. Huang, Y. M. Chiew, A three-dimensional continuum model incorporating static and kinetic effects for granular flows with applications to collapse of a two-dimensional granular column, Phys. Fluids 27 (11) (2015a) 113303, ISSN 10897666, doi:\let\@tempa\bibinfo@X@doi10.1063/1.4935626.

C. S. Campbell, Granular material flowsAn overview, Powder Technol. 162 (3) (2006) 208–229.

M. Pailha, M. Nicolas, O. Pouliquen, Initiation of underwater granular avalanches: Influence of the initial volume fraction, Phys. Fluids 20 (2008) 18–21, ISSN 10706631, doi:\let\@tempa\bibinfo@X@doi10.1063/1.3013896.

V. Topin, Y. Monerie, F. Perales, F. Radjaï, Collapse dynamics and runout of dense granular materials in a fluid, Phys. Rev. Lett. 109 (18) (2012) 188001, ISSN 00319007, doi:\let\@tempa\bibinfo@X@doi10.1103/PhysRevLett.109.188001.

L. Rondon, O. Pouliquen, P. Aussillous, Granular collapse in a fluid: role of the initial volume fraction, Phys. Fluids 23 (2011) 73301.

F. Bonnet, T. Richard, P. Philippe, Sensitivity to solid volume fraction of gravitational instability in a granular medium, Granul. Matter 12 (3) (2010) 317–325, ISSN 1434-5021, doi:\let\@tempa\bibinfo@X@doi10.1007/s10035-010-0178-7.

C. Meruane, a. Tamburrino, O. Roche, On the role of the ambient fluid on gravitational granular flow dynamics, J. Fluid Mech. 648 (2010) 381, ISSN 0022-1120, doi:\let\@tempa\bibinfo@X@doi10.1017/S0022112009993181.

C. Meruane, A. Tamburrino, O. Roche, Dynamics of dense granular flows of small-and-large-grain mixtures in an ambient fluid, Phys. Rev. E 86 (2) (2012) 026311, ISSN 1539-3755, doi:\let\@tempa\bibinfo@X@doi10.1103/PhysRevE.86.026311.

S. B. Savage, M. H. Babaei, T. Dabros, Modeling gravitational collapse of rectangular granular piles in air and water, Mech. Res. Commun. 56 (2014) 1–10, doi:\let\@tempa\bibinfo@X@doi10.1016/j.mechrescom.2013.11.001.

C.-H. Lee, Y. M. Low, Y.-M. Chiew, Multi-dimensional rheology-based two-phase model for sediment transport and applications to sheet flow and pipeline scour, Phys. Fluids 28 (2016) 053305, doi:\let\@tempa\bibinfo@X@doi10.1063/1.4948987.

B. M. Das, Principles of Geotechnical Engineering, Cengage Learning, Stamford, 2013.

J. Richardson, W. Zaki, Sedimentation and fluidisation: Part I, Chem. Eng. Res. Des. 32 (1954) S82–S100, ISSN 02638762, doi:\let\@tempa\bibinfo@X@doi10.1016/S0263-8762(97)80006-8.

Engelund, On the laminar and turbulent flows of ground water through homogeneous sand, Danish Academy of Technical Sciences, Copenhagen, 1953.

B. Camenen, Settling velocity of sediments at high concentrations, Coast. Eng. 51 (1) (2005) 91–100, ISSN 03783839, doi:\let\@tempa\bibinfo@X@doi10.1016/j.coastaleng.2003.12.004.

T.-J. Hsu, J. T. Jenkins, P. L.-F. Liu, On two-phase sediment transport: Dilute flow, J. Geophys. Res. 108, doi:\let\@tempa\bibinfo@X@doi10.1029/2001JC001276.

B. E. Launder, B. I. Sharma, Application of the energy-dissipation model of turbulence to the calculation of flow near a spinning disc, Lett. heat mass Transf. 1 (2) (1974) 131–137.

C. T. Crowe, On models for turbulence modulation in fluidparticle flows, Int. J. Multiph. Flow 26 (5) (2000) 719–727, doi:\let\@tempa\bibinfo@X@doi10.1016/S0301-9322(99)00050-6.

C.-H. Lee, Z. Huang, Y. M. Chiew, A multi-scale turbulent dispersion model for dilute flows with suspended sediment, Adv. Water Resour. 79 (2015b) 18–34, ISSN 03091708, doi:\let\@tempa\bibinfo@X@doi10.1016/j.advwatres.2015.02.002.

J. Hinze, Turbulence, Mc Graw Hill, New York, 1959.

T.-J. Hsu, J. T. Jenkins, P. L.-F. Liu, On two-phase sediment transport: sheet flow of massive particles, Proc. R. Soc. A Math. Phys. Eng. Sci. 460 (2048) (2004) 2223–2250, ISSN 1364-5021, doi:\let\@tempa\bibinfo@X@doi10.1098/rspa.2003.1273.

E. B. Pitman, L. Le, A two-fluid model for avalanche and debris flows., Philos. Trans. A. Math. Phys. Eng. Sci. 363 (1832) (2005) 1573–1601, ISSN 1364-503X, doi:\let\@tempa\bibinfo@X@doi10.1098/rsta.2005.1596.

N. Chien, Z. Wan, Mechanics of Sediment Transport, American Society of Civil Engineers, Reston, 1999.

F. White, Viscous fluid flow, McGraw-Hill, Singapore, ISBN 0071009957, 2000.

X. Yin, D. L. Koch, Hindered settling velocity and microstructure in suspensions of solid spheres with moderate Reynolds numbers, Phys. Fluids 19 (9) (2007) 093302, ISSN 10706631, doi:\let\@tempa\bibinfo@X@doi10.1063/1.2764109.

H. Burcharth, O. Andersen, On the One-Dimensional Steady and Unsteady Porous Flow Equation On the one-dimensional steady and unsteady porous flow equations, Coast. Eng. 24 (94) (1995) 233–257.

P. Higuera, J. L. Lara, I. J. Losada, Three-dimensional interaction of waves and porous coastal structures using OpenFOAM (R). Part I: Formulation and validation, Coast. Eng. 83 (2014) 243–258, doi:\let\@tempa\bibinfo@X@doi10.1016/j.coastaleng.2013.08.010.

H. Jasak, OpenFOAM: Open source CFD in research and industry, Inter. J. Nav. Arch. Oc. Engng. 1 (2009) 89–94.

OpenCFD, The Open Source CFD Toolbox: Programmer's Guide, 2014.

J. Towns, T. Cockerill, M. Dahan, I. Foster, K. Gaither, A. Grimshaw, V. Hazlewood, S. Lathrop, D. Lifk, G. D. Peterson, R. Roskies, J. R. Scott, N. Wilkins-Diehr, XSEDE: Accelerating Scientific Discovery, Comput Sci Eng 16 (5) (2014) 62–74, doi:\let\@tempa\bibinfo@X@doidoi:10.1109/MCSE.2014.80.

O. Roche, Y. Niño, A. Tamburrino, Pore fluid pressure and internal kinematics of gravitational laboratory air particle flows : Insights into the emplacement dynamics of pyroclastic flows, J. Geophys. Res. 115 (2010) 1–18, doi:\let\@tempa\bibinfo@X@doi10.1029/2009JB007133.

O. Pouliquen, C. Cassar, P. Jop, Y. Forterre, M. Nicolas, Flow of dense granular material: towards simple constitutive laws, J. Stat. Mech. 2006 (2006) P07020.

F. Chiodi, P. Claudin, B. Andreotti, A two-phase flow model of sediment transport: transition from bedload to suspended load, J. Fluid Mech. 755 (1967) (2014) 20, doi:\let\@tempa\bibinfo@X@doi10.1017/jfm.2014.422.

T. Revil-Baudard, J. Chauchat, A twophase model for sheet flow regime based on dense granular flow rheology, J. Geophys. Res. 118 (2013) 1–16.

D. B. Simons, M. L. Albertson, Uniform water conveyance channels in alluvial materials, J. Hydraul. Div. 86 (5) (1960) 33–71, ISSN 0044-796X.

P. Nielsen, Coastal Bottom Boundary Layers and Sediment Transport, World Scientific, Singapore, 1992.

D. M. Hanes, D. L. Inman, Experimental evaluation of a dynamic yield criterion for granular fluid flows, J. Geophys. Res. 90 (B5) (1985) 3670–3674, ISSN 2156-2202.

J. M. Sperry, J. J. Peirce, A model for estimating the hydraulic conductivity of granular material based on grain shape, grain size, and porosity, Ground Water 33 (6) (1995) 892–898, ISSN 0017-467X, doi:\let\@tempa\bibinfo@X@doi10.1111/j.1745-6584.1995.tb00033.x.

J. Bear, Dynamics of Fluids in Porous Media, American Elsevier, New York, ISBN 0486656756, doi:\let\@tempa\bibinfo@X@doi10.1097/00010694-197508000-00022, 1972.